

# Enhancing hyperspectral image unmixing with spatial correlations

Olivier Eches, Nicolas Dobigeon and Jean-Yves Tournieret

University of Toulouse, IRIT/INP-ENSEEIHT/TéSA

2 rue Camichel, 31071 Toulouse, France.

{Olivier.Eches, Nicolas.Dobigeon, Jean-Yves.Tournieret}@enseeiht.fr

## Abstract

This paper describes a new algorithm for hyperspectral image unmixing. Most of the unmixing algorithms proposed in the literature do not take into account the possible spatial correlations between the pixels. In this work, a Bayesian model is introduced to exploit these correlations. The image to be unmixed is assumed to be partitioned into regions (or *classes*) where the statistical properties of the abundance coefficients are homogeneous. A Markov random field is then proposed to model the spatial dependency of the pixels within any class. Conditionally upon a given class, the abundance vector is assumed to be *a priori* distributed according to a Gaussian distribution with unknown mean vector and covariance matrix that are characteristics of this class. This strategy is investigated for two well known mixing models: the linear mixing model and the normal compositional model. For both models, the posterior distributions of the unknown parameters and hyperparameters allow ones to infer the parameters of interest. These parameters include the abundances for each pixel, the means and variances of the abundances for each class, as well as a classification map indicating the classes of all pixels in the image. To overcome the complexity of the posterior distributions of interest, we consider Markov chain Monte Carlo methods that generate samples distributed according to these posteriors. The generated samples are then used for parameter and hyperparameter estimation. The accuracy of the proposed algorithms is illustrated on synthetic and real data.

## Index Terms

Bayesian inference, Monte Carlo methods, spectral unmixing, hyperspectral images, Markov random fields, Potts-Markov model.

## I. INTRODUCTION

Since the early 90's, hyperspectral imagery has been receiving growing interests in various fields of applications. For example, hyperspectral images have been recently used successfully for mapping the timber species in tropical forestry [1]. Hyperspectral image analysis involves many technical issues such as image classification, image segmentation, target detection and the crucial step of spectral unmixing. The problem of spectral unmixing has been investigated for several decades in both the signal processing and geoscience communities where many solutions have been proposed (see for instance [2] and [3] and references therein). Hyperspectral unmixing consists of decomposing the measured pixel reflectances into mixtures of pure spectra whose fractions are referred to as abundances. Assuming the image pixels are linear combinations of pure materials is very common in the unmixing framework. More precisely, the linear mixing model (LMM) considers the spectrum of a mixed pixel as a linear combination of endmembers [2]. Another statistical model known as normal compositional model (NCM) proposed by Stein in [4] assumes that the measured pixel reflectances are combinations of random endmembers (with known means) instead of deterministic ones. As illustrated in [5], the NCM can be preferred to the LMM when the image does not contain enough pure pixels.

Both LMM and NCM models require to have known endmember signatures. These signatures can be obtained from a spectral library or by using an endmember extraction algorithm (EEA). Some standard EEAs are reviewed in [6]. Once the endmembers that appear in a given image have been identified, the corresponding abundances have to be estimated in a so-called *inversion* step. Due to obvious physical considerations, the abundances (in LMM and NCM models) have to satisfy positivity and sum-to-one constraints. A lot of inversion algorithms respecting these constraints have been proposed in the literature. The fully constrained least squares (FCLS) [7] and scaled gradient (SGA) [8] algorithms are two optimization techniques that ensure the positivity and sum-to-one constraints inherent to the unmixing problem. Another interesting approach recently introduced in [9] consists of assigning appropriate prior distributions to the abundances and to solve the unmixing problem within a Bayesian framework. However, all these inversion strategies have been developed in a pixel by pixel context and, consequently, do not exploit the possible spatial correlations between the different pixels of the hyperspectral image. In this paper, we show that taking these spatial correlations into account allows one to improve the unmixing procedure. More

precisely, the Bayesian algorithms initially developed in [9] and [5] are modified to introduce spatial constraints between the abundance coefficients to be estimated.

Within a Bayesian estimation framework, a very popular strategy for modeling spatial information in an image is based on Markov random fields (MRFs). MRFs have been widely used in the image processing literature to properly describe neighborhood dependence between image pixels. MRFs and their pseudo-likelihood approximations have been introduced by Besag in [10]. MRFs have then been popularized by Geman in [11] by exploiting the Gibbs distribution inherent to MRFs. MRFs have also been proposed to analyze hyperspectral data for image segmentation [12]–[14] or for blind source separation [15]. This paper proposes to study the interest of using MRFs for unmixing hyperspectral images. More precisely, the two Bayesian unmixing strategies (based on the LMM and NCM models) developed in [9] and [5] are generalized to take into account spatial correlations between the pixels of an hyperspectral image. The hyperspectral image to be analyzed is assumed to be partitioned into homogeneous regions (or classes) in which the abundance vectors have the same first and second order statistics (means and covariances). This assumption implies an implicit image classification, modeled by hidden labels whose spatial dependencies follow a Potts-Markov field [16]. Conditionally upon these labels, the abundance vectors are assigned appropriate prior distributions with unknown means and variances that depend on the pixel class. These prior distributions ensure the positivity and sum-to-one constraints of the abundance coefficients. They are based on a reparametrization of the abundance vectors and are much more flexible than the priors previously studied in [9], [5] or [17]. Of course, the accuracy of the abundance estimation procedure drastically depends on the hyperparameters associated to these priors. This paper proposes to estimate these hyperparameters in a fully unsupervised manner by introducing a second level of hierarchy in the Bayesian inference. Non-informative prior distributions are assigned to the hyperparameters. The unknown parameters (labels and abundance vectors) and hyperparameters (prior abundance mean and variance for each class) are then inferred from their joint posterior distribution. Since this posterior is too complex to derive closed-form expressions for the classical Bayesian estimators, Markov chain Monte Carlo (MCMC) techniques are studied to alleviate the numerical problems related to the NCM and LMM with spatial constraints. MCMC generate samples asymptotically distributed according to the joint posterior of interest. These samples are finally used to approximate the Bayesian estimators, such as the minimum mean square error (MMSE) or the maximum *a posteriori* estimators. Note that the underlying classification and abundance estimation problems are jointly solved

within this Bayesian framework.

The paper is organized as follows. The unmixing problem associated to the LMM and NCM with spatial correlations is formulated in II. Section III introduces a hierarchical Bayesian model appropriate to this unmixing problem. The MCMC algorithms required to approximate the Bayesian LMM and NCM estimators are described in Section IV. Simulation results conducted on simulated and real data are provided in Sections V and VI. Finally, the conclusions of this work are given in Section VII.

## II. TECHNICAL BACKGROUND AND PROBLEM FORMULATION

### A. Unmixing statistical models

As highlighted in the previous section, two linear models have been mainly proposed in the remote sensing literature for spectral unmixing. The LMM assumes that the spectrum of a given pixel is a linear combination of deterministic endmembers corrupted by an additive white Gaussian noise [2]. More specifically, according to the LMM, the observed  $L$ -spectrum of a given pixel  $p$  is defined as

$$\mathbf{y}_p = \mathbf{M}\mathbf{a}_p + \mathbf{n}_p \quad (1)$$

where  $L$  is the number of spectral bands,  $\mathbf{M} = [\mathbf{m}_1, \dots, \mathbf{m}_R]$  is a known  $L \times R$  matrix containing the  $L$ -spectra of the endmembers,  $\mathbf{a}_p$  is the  $R \times 1$  abundance vector,  $R$  is the number of endmembers that are present in the image and  $\mathbf{n}_p$  is the noise vector. The vector  $\mathbf{n}_p$  is classically assumed to be an independent and identically distributed (i.i.d.) zero-mean Gaussian sequence with unknown variance  $s_p^2$

$$\mathbf{n}_p | s_p^2 \sim \mathcal{N}(\mathbf{0}_L, s_p^2 \mathbf{I}_L) \quad (2)$$

where  $\mathbf{I}_L$  is the  $L \times L$  identity matrix.

Conversely, the NCM assumes the endmembers are random vectors with known means [4]. The NCM has shown interesting properties for the unmixing of hyperspectral images that do not contain enough pure pixels, as illustrated in [5]. According to the NCM, the observed  $L$ -spectrum of a given pixel  $p$  is defined as

$$\mathbf{y}_p = \mathbf{E}_p \mathbf{a}_p$$

where  $\mathbf{E}_p = [\mathbf{e}_{p,1}, \dots, \mathbf{e}_{p,R}]$  is the  $L \times R$  matrix of random endmember spectra that differ from one pixel to another. The different endmember random vectors  $\mathbf{e}_{p,r}$  ( $r = 1, \dots, R$ ,  $p = 1, \dots, P$ ) are independent Gaussian vectors with known means  $\mathbf{m}_r$  (common for all

the pixels), and an unknown diagonal covariance matrix  $w_p^2 \mathbf{I}_L$  (different from one pixel to another)

$$\mathbf{e}_{p,r} | w_p^2 \sim \mathcal{N}(\mathbf{m}_r, w_p^2 \mathbf{I}_L). \quad (3)$$

For both models, considering an image of  $P$  pixels, standard matrix notations can be adopted leading to  $\mathbf{Y} = [\mathbf{y}_1, \dots, \mathbf{y}_P]$  and  $\mathbf{A} = [\mathbf{a}_1, \dots, \mathbf{a}_P]$ .

### B. Introducing spatial dependencies between abundances

We propose in this paper to exploit some spatial correlations between the pixels of the hyperspectral image to be analyzed. More precisely, when performing unmixing, it is interesting to consider that the abundances of a given pixel are similar to the abundances of its neighboring pixels. Formally, the hyperspectral image is assumed to be partitioned into  $K$  regions or *classes*. Let  $\mathcal{I}_k \subset \{1, \dots, P\}$  denote the subset of pixel indexes belonging to the  $k$ th class. A label vector of size  $P \times 1$  denoted as  $\mathbf{z} = [z_1, \dots, z_P]^T$  with  $z_p \in \{1, \dots, K\}$  is introduced to identify the class to which each pixel  $p$  belongs ( $p = 1, \dots, P$ ). In other terms

$$z_p = k \Leftrightarrow p \in \mathcal{I}_k. \quad (4)$$

In each class, the abundance vectors to be estimated are assumed to share the same first and second order statistics, i.e.,  $\forall k \in \{1, \dots, K\}, \forall (p, p') \in \mathcal{I}_k \times \mathcal{I}_k$

$$\begin{aligned} \mathbb{E}[\mathbf{a}_p] &= \mathbb{E}[\mathbf{a}_{p'}] = \boldsymbol{\mu}_k \\ \mathbb{E}[(\mathbf{a}_p - \boldsymbol{\mu}_k)(\mathbf{a}_p - \boldsymbol{\mu}_k)^T] &= \mathbb{E}[(\mathbf{a}_{p'} - \boldsymbol{\mu}_k)(\mathbf{a}_{p'} - \boldsymbol{\mu}_k)^T]. \end{aligned} \quad (5)$$

Therefore, the  $k$ th class of the hyperspectral image to be unmixed is fully characterized by the abundance mean vector  $\boldsymbol{\mu}_k$  and the abundance covariance matrix of the pixels belonging to this class.

### C. Markov random fields

To describe spatial constraints between pixels, it is important to properly define a neighborhood structure. The neighborhood relation between two pixels  $i$  and  $j$ , has to be symmetric: if  $i$  is a neighbor of  $j$  then  $j$  is a neighbor of  $i$ . This relation is applied to the nearest neighbors of the considered pixel, for example the fourth, eighth or twelfth nearest pixels. Fig. 1 shows two examples of neighborhood structures. The four pixel structure or *1-order neighborhood* will be considered in the rest of the paper. Therefore, the associated set of

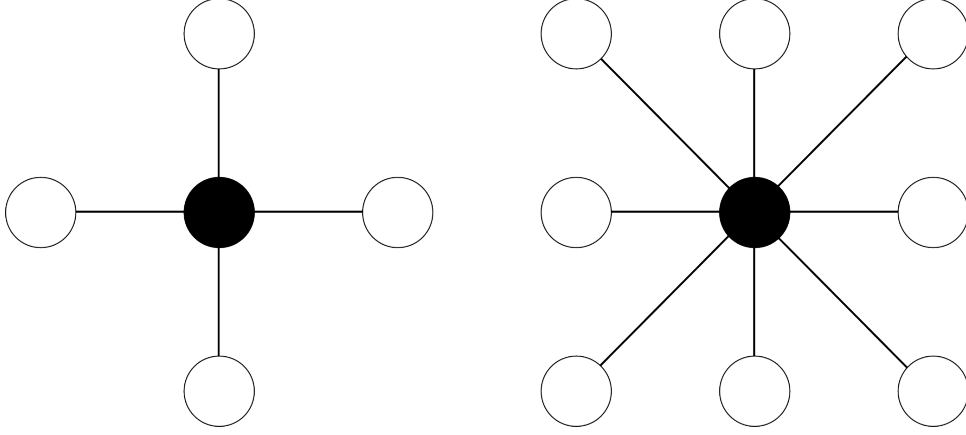


Fig. 1. 4-pixel (left) and 8-pixel (right) neighborhood structures. The considered pixel appear as a black circle whereas its neighbors are depicted in white.

neighbors, or *cliques*, has only vertical and horizontal possible configurations (see [10], [11] for more details).

Once the neighborhood structure has been clearly established, the MRF can be easily defined. Let  $z_p$  denote a random variable associated to the  $p$ th pixel of an image of  $P$  pixels. In our context of hyperspectral image unmixing, these variables will refer to the class to which the pixels belong and take their values in a finite set, e.g.,  $\{1, \dots, K\}$ . The whole set of random variables  $\{z_1, \dots, z_P\}$  forms a random field. An MRF is then defined when the conditional distribution of  $z_i$  given the other pixels  $\mathbf{z}_{-i}$  only depend on its neighbors  $\mathbf{z}_{\mathcal{V}(i)}$ , i.e.,

$$f(z_i | \mathbf{z}_{-i}) = f(z_i | \mathbf{z}_{\mathcal{V}(i)}) \quad (6)$$

where  $\mathcal{V}(i)$  is the neighborhood structure considered and  $\mathbf{z}_{-i} = \{z_j; j \neq i\}$ .

Since the pioneer work of Geman [11], MRFs have been widely used in the image processing community as in [18], [19]. The hyperspectral community has also recently exploited the advantages of MRFs for hyperspectral image analysis [20], [14] and [15]. However, to our knowledge, MRFs have not been studied for hyperspectral image unmixing. MRFs provide an efficient way of modeling correlations between pixels, which is adapted to the intrinsic properties of most images. Two specific MRFs are appropriate for image analysis: the Ising model for binary random variables and the Potts-Markov model that is a simple generalization to more-than-two variables [16]. This paper focuses on the Potts-Markov model since it is very appropriate to hyperspectral image segmentation [15]. Given a discrete random field  $\mathbf{z}$  attached to an image with  $P$  pixels, the Hammersley-Clifford theorem

yields

$$f(\mathbf{z}) = \frac{1}{G(\beta)} \exp \left[ \sum_{p=1}^P \sum_{p' \in \mathcal{V}(p)} \beta \delta(z_p - z_{p'}) \right] \quad (7)$$

where  $\beta$  is the *granularity* coefficient,  $G(\beta)$  is the normalizing constant or *partition function* [21] and  $\delta(\cdot)$  is the Kronecker function

$$\delta(x) = \begin{cases} 1, & \text{if } x = 0, \\ 0, & \text{otherwise.} \end{cases}$$

Note that drawing a label vector  $\mathbf{z} = [z_1, \dots, z_P]$  from the distribution (7) can be easily achieved without knowing  $G(\beta)$  by using a Gibbs sampler (the corresponding algorithmic scheme is summarized in Algo. 1). However, a major difficulty with the distribution (7) comes from the partition function that has no closed-form expression and depends on the unknown hyperparameter  $\beta$ . The hyperparameter  $\beta$  tunes the degree of homogeneity of each region in the image. Some simulations have been conducted to show the influence of this parameter on image homogeneity. Synthetic images have been generated from a Potts-Markov model with  $K = 3$  (corresponding to three gray levels in the image) and a 1-order neighborhood structure. Fig. 2 indicates that a small value of  $\beta$  induces a *noisy* image with a large number of regions, contrary to a large value of  $\beta$  that leads to few and large homogeneous regions. Note that it is unnecessary to consider values of  $\beta \geq 2$  since “When  $\beta \geq 2$ , the Potts-Markov model is almost surely concentrated on single-color images” [22, p. 237]. In this work, the granularity coefficient  $\beta$  will be fixed *a priori*. However, it is interesting to mention that the estimation of  $\beta$  might also be conducted by using the methods studied in [23], [24] and [25].

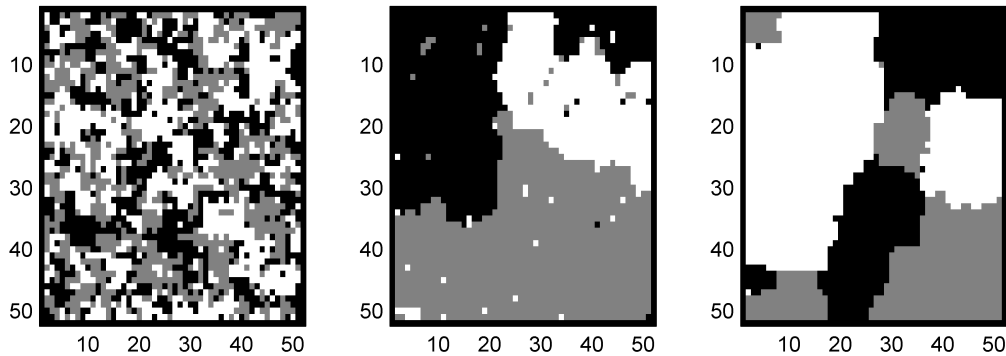


Fig. 2. Synthetic images generated from a Potts-Markov model with (from left to right)  $\beta = 0.8, 1.4, 2$ .

---

**Algorithm 1** MRF Simulation

---

- 1: **for**  $n = 1$  to  $N_{\text{MC}}$  **do**
- 2:   **for**  $p = 1$  to  $P$  **do**
- 3:     **for**  $k = 1$  to  $K$  **do**
- 4:       Compute  $w_k \propto \text{P}[z_p = k | \mathbf{z}_{-p}]$  according to (7)
- 5:     **end for**
- 6:   Compute the normalizing constant

$$G(\beta) = \sum_{k=1}^K w_k$$

- 7:   Set the probability vector

$$\tilde{\mathbf{w}} = \left[ \frac{w_1}{G(\beta)}, \dots, \frac{w_K}{G(\beta)} \right]$$

- 8:   Draw  $z_p$  in  $\{1, \dots, K\}$  with proba.  $\{\tilde{w}_1, \dots, \tilde{w}_K\}$ .
  - 9:   **end for**
  - 10: **end for**
- 

#### D. Abundance Reparametrization

As explained before, the fraction vectors  $\mathbf{a}_p$  should satisfy positivity and sum-to-one constraints defined as

$$\begin{cases} a_r \geq 0, \forall r = 1, \dots, R, \\ \sum_{r=1}^R a_r = 1. \end{cases} \quad (8)$$

We have recently proposed to handle these constraints within a Bayesian framework (for hyperspectral image unmixing) by considering an abundance prior uniformly distributed on an appropriate simplex (satisfying the set of constraints) [9], [17]. However, we have noticed that this uniform distribution is not sufficiently flexible to allow an efficient image partitioning resulting from MRF theory. Therefore, we have considered a more flexible distribution able to have different shapes characterizing the classes within the image. More precisely, we have considered a reparametrization for positive parameters constrained to sum-to-one introduced in [26] for a pharmacokinetic problem and recently applied to hyperspectral unmixing in [27]. It consists of rewriting the abundances as a function of random variables that will be referred to as *logistic coefficients* in the rest of the paper. A logistic coefficient vector



$\mathbf{t}_p = [t_{1,p} \dots, t_{R,p}]^T$  is assigned to each abundance vector  $\mathbf{a}_p$ , according to the relationship

$$a_{r,p} = \frac{\exp(t_{r,p})}{\sum_{r=1}^R \exp(t_{r,p})}. \quad (9)$$

Initially, the spatial dependencies resulting from the image partitioning described in II-B are based on the first and second order statistics of the abundance vectors  $\mathbf{a}_p$ . However, the spatial constraints defined in (5) can be easily adapted when using logistic coefficient vectors. Indeed, in each class, the unknown logistic coefficient vectors are assumed to share the same first and second order statistics, i.e.,

$$\begin{aligned} \mathbb{E}[\mathbf{t}_p] &= \mathbb{E}[\mathbf{t}_{p'}] = \boldsymbol{\psi}_k \\ \mathbb{E}\left[(\mathbf{t}_p - \boldsymbol{\psi}_k)(\mathbf{t}_p - \boldsymbol{\psi}_k)^T\right] &= \mathbb{E}\left[(\mathbf{t}_{p'} - \boldsymbol{\psi}_k)(\mathbf{t}_{p'} - \boldsymbol{\psi}_k)^T\right] \\ &= \boldsymbol{\Sigma}_k. \end{aligned} \quad (10)$$

With this reparametrization, the  $k$ th class is fully characterized by the unknown hyperparameters  $\boldsymbol{\psi}_k$  and  $\boldsymbol{\Sigma}_k$ .

### III. HIERARCHICAL BAYESIAN MODEL

This section investigates the likelihoods and the priors inherent to the NCM and LMM for the spectral unmixing of hyperspectral images, based on Potts-Markov random fields and logistic coefficients.

#### A. Unknown parameters

We first properly define the unknown parameter vectors associated to the LMM and NCM unmixing strategies

$$\boldsymbol{\Theta}_{\text{LMM}} = \{\mathbf{T}, \mathbf{z}, \mathbf{s}\}$$

$$\boldsymbol{\Theta}_{\text{NCM}} = \{\mathbf{T}, \mathbf{z}, \mathbf{w}\}$$

where  $\mathbf{s} = [s_1^2, \dots, s_P^2]^T$  and  $\mathbf{w} = [w_1^2, \dots, w_P^2]^T$  are the noise and endmember variance vectors,  $\mathbf{z}$  is the label vector and  $\mathbf{T} = [\mathbf{t}_1, \dots, \mathbf{t}_P]$  with  $\mathbf{t}_p = [t_{1,p}, \dots, t_{R,p}]^T$  ( $p = 1, \dots, P$ ) is the logistic coefficient matrix used for the abundance reparametrization.

#### B. Likelihood functions

This section summarizes the likelihoods corresponding to the LMM and NCM.

1) *LMM likelihood*: The additive white Gaussian noise sequence of the LMM allows one to write<sup>1</sup>  $\mathbf{y}_p | \mathbf{t}_p, s_p^2 \sim \mathcal{N}(\mathbf{M}\mathbf{a}_p(\mathbf{t}_p), s_p^2 \mathbf{I}_L)$  ( $p = 1, \dots, P$ ). Therefore the likelihood function

<sup>1</sup>Note that the dependence of the abundance vector  $\mathbf{a}_p$  on the logistic coefficient vector  $\mathbf{t}_p$  through (9) has been explicitly mentioned by denoting  $\mathbf{a}_p = \mathbf{a}_p(\mathbf{t}_p)$ .

of  $\mathbf{y}_p$  can be expressed as

$$f_{\text{LMM}}(\mathbf{y}_p | \mathbf{t}_p, s_p^2) = \left( \frac{1}{2\pi s_p^2} \right)^{\frac{L}{2}} \exp \left[ -\frac{\|\mathbf{y}_p - \mathbf{M}\mathbf{a}_p(\mathbf{t}_p)\|^2}{2s_p^2} \right] \quad (11)$$

where  $\|\mathbf{x}\| = \sqrt{\mathbf{x}^T \mathbf{x}}$  is the standard  $\ell^2$  norm. By assuming independence between the noise sequences  $\mathbf{n}_p$  ( $p = 1, \dots, P$ ), the likelihood of the  $P$  image pixels is

$$f_{\text{LMM}}(\mathbf{Y} | \mathbf{T}, \mathbf{s}) = \prod_{p=1}^P f_{\text{LMM}}(\mathbf{y}_p | \mathbf{t}_p, s_p^2). \quad (12)$$

2) *NCM likelihood*: As stated in paragraph II-D, according to the NCM, the endmember spectra  $\mathbf{e}_{p,r}$  ( $r = 1, \dots, R$ ,  $p = 1, \dots, P$ ) are Gaussian vectors with mean vectors  $\mathbf{m}_r$  and covariance matrices  $w_p^2 \mathbf{I}_L$  that can change from one pixel  $p$  to another. Thus, the likelihood of the observed pixel  $\mathbf{y}_p$  for the NCM can be written as

$$f_{\text{NCM}}(\mathbf{y}_p | \mathbf{t}_p, w_p^2) = \frac{1}{[2\pi w_p^2 c(\mathbf{t}_p)]^{\frac{L}{2}}} \exp \left[ -\frac{\|\mathbf{y}_p - \boldsymbol{\mu}(\mathbf{t}_p)\|^2}{2w_p^2 c(\mathbf{t}_p)} \right] \quad (13)$$

with

$$\boldsymbol{\mu}(\mathbf{t}_p) = \sum_{r=1}^R \mathbf{m}_r a_{r,p}(\mathbf{t}_p), \quad c(\mathbf{t}_p) = \sum_{r=1}^R a_{r,p}(\mathbf{t}_p)^2.$$

Assuming the prior independence between the observed spectrum pixels, the likelihood function of the  $P$  image pixels is

$$f_{\text{NCM}}(\mathbf{Y} | \mathbf{T}, \mathbf{w}) = \prod_{p=1}^P f_{\text{NCM}}(\mathbf{y}_p | \mathbf{t}_p, w_p^2). \quad (14)$$

### C. Parameter priors

This section introduces the prior distributions of the unknown parameters and their associated hyperparameters that will be used for the LMM and NCM. The directed acyclic graph (DAG) for the parameter priors and hyperpriors for the two statistical models is represented in Fig. 3.

1) *Label prior*: The prior distribution for the label vector  $\mathbf{z} = [z_1, \dots, z_P]^T$  introduced in paragraph II-C is a Potts-Markov random field with a 1-order neighborhood and a known granularity coefficient  $\beta$  (fixed *a priori*). The resulting prior distribution can be written

$$f(\mathbf{z}) \propto \exp \left[ \sum_{p=1}^P \sum_{p' \in \mathcal{V}(p)} \beta \delta(z_p - z_{p'}) \right] \quad (15)$$

where  $\mathcal{V}(p)$  is the 1-order neighborhood depicted in Fig. 1 and  $\propto$  means “proportional to.” Note that the 4-connexity clique considered in this paper allows one to split the image into

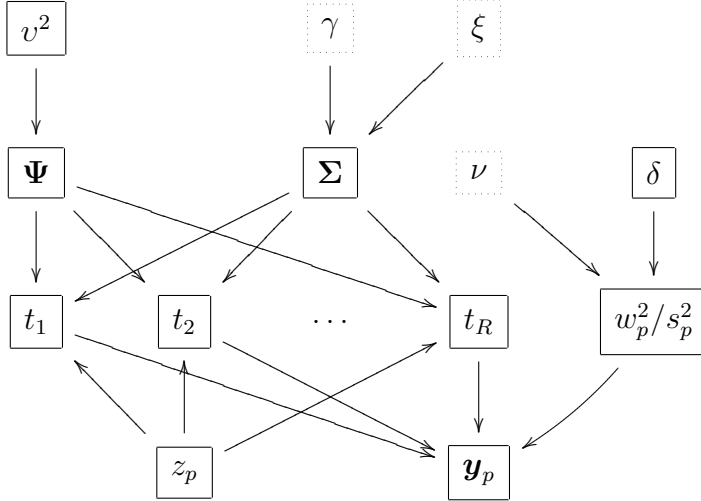


Fig. 3. DAG for the parameter priors and hyperpriors (the fixed parameters appear in dashed boxes) for the LMM and NCM.

two sets of so-called “black” and “white” sites, like a chessboard. Consequently, (15) can be reformulated in the classical way

$$f(\mathbf{z}) \propto \exp \left[ \sum_{p \in \mathcal{D}_w} \sum_{p' \in \mathcal{V}(p)} \beta \delta(z_p - z_{p'}) \right] \exp \left[ \sum_{p \in \mathcal{D}_b} \sum_{p' \in \mathcal{V}(p)} \beta \delta(z_p - z_{p'}) \right] \quad (16)$$

where  $\mathcal{D}_w$  (resp.  $\mathcal{D}_b$ ) is the set of indexes associated to the white (resp. black) sites.

2) *Logistic coefficient prior*: Following the approach described in paragraph II-B, each component of  $\mathbf{t}_p$  is assumed to be distributed according to a Gaussian distribution. In addition, as highlighted in II-D (see (10)), the mean and variance of the logistic coefficients depend on the class to which the corresponding pixel belong. Therefore, the prior distribution for the  $\mathbf{t}_p$  is explicitly defined conditionally upon the pixel label

$$t_{r,p} | z_p = k, \psi_{r,k}, \sigma_{r,k}^2 \sim \mathcal{N}(\psi_{r,k}, \sigma_{r,k}^2) \quad (17)$$

where the hyperparameters  $\psi_{r,k}$  and  $\sigma_{r,k}^2$  depend on the associated pixel class  $k$ . As suggested in Section I, a hierarchical Bayesian algorithm will be used to estimate these hyperparameters. For a given pixel  $p$ , by assuming prior independence between the coefficients  $t_{1,p}, \dots, t_{R,p}$ , the prior distribution for the vector  $\mathbf{t} = [t_{1,p}, \dots, t_{R,p}]^T$  is

$$f(\mathbf{t}_p | z_p = k, \boldsymbol{\psi}_k, \boldsymbol{\Sigma}_k) \sim \mathcal{N}(\boldsymbol{\psi}_k, \boldsymbol{\Sigma}_k) \quad (18)$$

where  $\boldsymbol{\psi}_k = [\psi_{1,k}, \dots, \psi_{R,k}]^T$  and  $\boldsymbol{\Sigma}_k = \text{diag}(\sigma_{r,k}^2)$  is the  $R \times R$  diagonal matrix whose diagonal elements are  $\sigma_{r,k}^2$ .

By assuming prior independence between the  $P$  vectors  $\mathbf{t}_1, \dots, \mathbf{t}_P$ , the full posterior distribution for the logistic coefficient matrix  $\mathbf{T}$  is

$$f(\mathbf{T}|\Psi, \Sigma) = \prod_{k=1}^K \prod_{p \in \mathcal{I}_k} f(\mathbf{t}_p | z_p = k, \psi_k, \Sigma_k) \quad (19)$$

with  $\Psi = [\psi_1, \dots, \psi_K]$  and  $\Sigma = \{\Sigma_1, \dots, \Sigma_K\}$ .

3) *Noise and endmember variance priors:* Conjugate inverse-gamma distributions are assigned to the noise and endmember variances leading to

$$\begin{aligned} w_p^2 | \nu, \delta &\sim \mathcal{IG}(\nu, \delta) \\ s_p^2 | \nu, \delta &\sim \mathcal{IG}(\nu, \delta) \end{aligned} \quad (20)$$

where  $\nu$  and  $\delta$  are adjustable hyperparameters. This paper assumes  $\nu = 1$  (as in [28] or [29]) and estimates  $\delta$  jointly with the other unknown parameters and hyperparameters (using a hierarchical Bayesian algorithm).

By assuming independence between the different variance priors and by denoting  $\mathbf{w} = [w_1^2, \dots, w_P^2]^T$  and  $\mathbf{s} = [s_1^2, \dots, s_P^2]^T$ , the prior distributions for  $\mathbf{w}$  and  $\mathbf{s}$  can be written

$$f(\mathbf{w}|\delta) = \prod_{p=1}^P f(w_p^2|\delta) \quad (21)$$

and

$$f(\mathbf{s}|\delta) = \prod_{p=1}^P f(s_p^2|\delta). \quad (22)$$

#### D. Hyperparameter priors

Hierarchical Bayesian algorithms require to define prior distributions for the hyperparameters. A particular attention has been devoted to the hyperparameters  $\psi_{r,k}$  and  $\sigma_{r,k}^2$  as they fully describe the different classes partitioning the image. The prior distributions for  $\psi_{r,k}$  and  $\sigma_{r,k}^2$  are conjugate distributions. More precisely, a vague inverse-gamma distribution is chosen for the logistic coefficient variance  $\sigma_{r,k}^2$ , i.e.,

$$\sigma_{r,k}^2 | \xi, \gamma \sim \mathcal{IG}(\xi, \gamma) \quad (23)$$

where  $\xi$  and  $\gamma$  have been tuned to  $\xi = 1$  and  $\gamma = 5$  (in order to obtain a large variance). Moreover, a centered Gaussian distribution with unknown variance has been chosen as prior for the logistic coefficient mean

$$\psi_{r,k} | v^2 \sim \mathcal{N}(0, v^2) \quad (24)$$

where  $v^2$  is another adjustable hyperparameter. By assuming independence between the different mean vectors  $\boldsymbol{\psi}_k$ , ( $k = 1, \dots, K$ ), as well as between the covariance matrices  $\boldsymbol{\Sigma}_k$ , ( $k = 1, \dots, K$ ), the full priors for the two hyperparameters  $\boldsymbol{\Psi}$  and  $\boldsymbol{\Sigma}$  can be expressed as

$$f(\boldsymbol{\Psi}|v^2) \propto \prod_{k=1}^K \prod_{r=1}^R \left(\frac{1}{v^2}\right)^{\frac{1}{2}} \exp\left(-\frac{\psi_{r,k}^2}{2v^2}\right) \quad (25)$$

$$f(\boldsymbol{\Sigma}|\xi, \gamma) \propto \prod_{k=1}^K \prod_{r=1}^R \frac{\gamma^\xi}{\Gamma(\xi)} (\sigma_{r,k}^2)^{-(\xi+1)} \exp\left(-\frac{\gamma}{\sigma_{r,k}^2}\right). \quad (26)$$

Jeffreys' priors are chosen for the hyperparameters  $\delta$  and  $v^2$

$$f(\delta) \propto \frac{1}{\delta} \mathbf{1}_{\mathbb{R}^+}(\delta), \quad f(v^2) \propto \frac{1}{v^2} \mathbf{1}_{\mathbb{R}^+}(v^2). \quad (27)$$

reflecting the lack of knowledge regarding these two hyperparameters. As this last hierarchy level within the Bayesian inference, the hyperparameter vector can be defined as  $\Omega = \{\boldsymbol{\Psi}, \boldsymbol{\Sigma}, v^2, \delta\}$ .

#### E. Joint distribution

The joint posterior distribution of the unknown parameters and hyperparameters is classically defined using the hierarchical structure

$$f(\boldsymbol{\Theta}, \Omega | \mathbf{Y}) = f(\mathbf{Y} | \boldsymbol{\Theta}) f(\boldsymbol{\Theta} | \Omega) f(\Omega). \quad (28)$$

Straightforward computations yield the following posteriors for the LMM and NCM

$$\begin{aligned} f(\boldsymbol{\Theta}_{\text{LMM}}, \Omega | \mathbf{Y}) &\propto \prod_{p=1}^P \left(\frac{1}{s_p^2}\right)^{\frac{L}{2}} \exp\left[-\frac{\|\mathbf{y}_p - \mathbf{M}\mathbf{a}_p(\mathbf{t}_p)\|^2}{2s_p^2}\right] \exp\left[\sum_{p=1}^P \sum_{p' \in \mathcal{V}(p)} \beta \delta(z_p - z_{p'})\right] \\ &\times \delta^{P-1} \prod_{p=1}^P \left(\frac{1}{w_p^2}\right)^{\nu+1} \exp\left(-\frac{\delta}{w_p^2}\right) \left(\frac{1}{v^2}\right)^{\frac{RK}{2}+1} \\ &\times \prod_{r,k} \frac{1}{\sigma_{r,k}^{n_k+1}} \exp\left[-\left(\frac{\psi_{r,k}^2}{2v^2} + \frac{2\gamma + \sum_{p \in \mathcal{I}_k} (t_{r,p} - \psi_{r,k})^2}{2\sigma_{r,k}^2}\right)\right] \end{aligned} \quad (29)$$

and

$$\begin{aligned} f(\boldsymbol{\Theta}_{\text{NCM}}, \Omega | \mathbf{Y}) &\propto \prod_{p=1}^P \frac{1}{[w_p^2 c(\mathbf{t}_p)]^{L/2}} \exp\left[-\sum_{p=1}^P \frac{\|\mathbf{y}_p - \boldsymbol{\mu}(\mathbf{t}_p)\|^2}{2w_p^2 c(\mathbf{t}_p)}\right] \exp\left[\sum_{p=1}^P \sum_{p' \in \mathcal{V}(p)} \beta \delta(z_p - z_{p'})\right] \\ &\times \delta^{P-1} \prod_{p=1}^P \left(\frac{1}{w_p^2}\right)^{\nu+1} \exp\left(-\frac{\delta}{w_p^2}\right) \left(\frac{1}{v^2}\right)^{\frac{RK}{2}+1} \\ &\times \prod_{r,k} \frac{1}{\sigma_{r,k}^{n_k+1}} \exp\left[-\left(\frac{\psi_{r,k}^2}{2v^2} + \frac{2\gamma + \sum_{p \in \mathcal{I}_k} (t_{r,p} - \psi_{r,k})^2}{2\sigma_{r,k}^2}\right)\right] \end{aligned} \quad (30)$$

with  $n_k = \text{card}(\mathcal{I}_k)$ . The posterior distributions associated to the LMM and NCM are too complex to obtain closed-form expressions for the MMSE or MAP estimators of the unknown parameter vector  $\Theta$ . To alleviate this problem, we propose to use MCMC methods to generate samples that are asymptotically distributed according to the posterior of interest. The generated samples are then used to approximate the Bayesian estimators. The next section studies hybrid Gibbs samplers that generate samples asymptotically distributed according to the posterior distributions (30) or (29).

#### IV. HYBRID GIBBS SAMPLERS

This section studies Metropolis-within-Gibbs samplers that generate samples according to the joint posterior  $f(\Theta, \Omega | \mathbf{Y})$ . The algorithms used for the NCM and LMM are respectively summarized in Algo. 2 and Algo. 3. The Gibbs sampler iteratively generates samples distributed according to the conditional distributions detailed below.

##### A. Conditional distribution of the label vector $\mathbf{z}$

For each pixel  $p$  ( $p = 1, \dots, P$ ), the class label  $z_p$  is a discrete random variable whose conditional distribution is fully characterized by the probabilities

$$\mathbb{P}[z_p = k | \mathbf{z}_{-p}, \mathbf{t}_p, \boldsymbol{\psi}_k, \boldsymbol{\Sigma}_k] \propto f(\mathbf{t}_p | z_p = k, \boldsymbol{\psi}_k, \boldsymbol{\Sigma}_k) f(z_p | \mathbf{z}_{-p}) \quad (31)$$

where  $k = 1, \dots, K$  ( $K$  is the number of classes) and  $\mathbf{z}_{-p}$  denotes the vector  $\mathbf{z}$  whose  $p$ th element has been removed. These posterior probabilities can be expressed as

$$\begin{aligned} \mathbb{P}[z_p = k | \mathbf{z}_{-p}, \mathbf{t}_p, \boldsymbol{\psi}_k, \boldsymbol{\Sigma}_k] &\propto |\boldsymbol{\Sigma}_k|^{-1/2} \exp \left[ -\frac{1}{2} (\mathbf{t}_p - \boldsymbol{\psi}_k)^T \boldsymbol{\Sigma}_k^{-1} (\mathbf{t}_p - \boldsymbol{\psi}_k) \right] \\ &\times \exp \left[ \sum_{p=1}^P \sum_{p' \in \mathcal{V}(p)} \beta \delta(z_p - z_{p'}) \right] \end{aligned} \quad (32)$$

where  $|\boldsymbol{\Sigma}_k| = \prod_{r=1}^R \sigma_{r,k}^2$ . Note that the posterior probabilities of the label vector  $\mathbf{z}$  in (32) define an MRF. Consequently, sampling from this conditional distribution can be achieved using the scheme detailed in Algo. 1, i.e., by drawing a discrete value in the finite set  $\{1, \dots, K\}$  with the probabilities (32). By using the factorized form (16) of the prior distribution for  $\mathbf{z}$ , a Gibbs sampler is proposed to successively generate  $z_p$  for  $p \in \mathcal{D}_w$  and then for  $p \in \mathcal{D}_b$  (where  $\mathcal{D}_w$  and  $\mathcal{D}_b$  have been defined in paragraph III-C1).

### B. Conditional distribution of logistic coefficient matrix $\mathbf{T}$

For each pixel  $p$ , the Bayes theorem yields

$$f(\mathbf{t}_p | z_p = k, \boldsymbol{\psi}_k, \boldsymbol{\Sigma}_k, \mathbf{y}_p) \propto f(\mathbf{y}_p | \mathbf{t}_p) f(\mathbf{t}_p | \boldsymbol{\psi}_k, \boldsymbol{\Sigma}_k).$$

This conditional distribution depending on the likelihood function, two cases will be investigated<sup>2</sup>.

1) *LMM*: For a given pixel  $p$ , the conditional distribution of  $\mathbf{t}_p$  is

$$\begin{aligned} f(\mathbf{t}_p | z_p = k, \boldsymbol{\psi}_k, \boldsymbol{\Sigma}_k, \mathbf{y}_p, s_p^2) &\propto \left(\frac{1}{s_p^2}\right)^{\frac{L}{2}} \exp\left\{-\frac{1}{2s_p^2} \|\mathbf{y}_p - \mathbf{M}\mathbf{a}_p(\mathbf{t}_p)\|^2\right\} \\ &\times |\boldsymbol{\Sigma}_k|^{-\frac{1}{2}} \exp\left[-\frac{1}{2} (\mathbf{t}_p - \boldsymbol{\psi}_k)^T \boldsymbol{\Sigma}_k^{-1} (\mathbf{t}_p - \boldsymbol{\psi}_k)\right]. \end{aligned} \quad (33)$$

2) *NCM*: The conditional distribution of  $\mathbf{t}_p$  for each pixel is given by

$$\begin{aligned} f(\mathbf{t}_p | z_p = k, \boldsymbol{\psi}_k, \boldsymbol{\Sigma}_k, \mathbf{y}_p, w_p^2) &\propto \frac{1}{[w_p^2 c(\mathbf{t}_p)]^{L/2}} \exp\left\{-\frac{1}{2w_p^2 c(\mathbf{t}_p)} \|\mathbf{y}_p - \boldsymbol{\mu}(\mathbf{t}_p)\|^2\right\} \\ &\times |\boldsymbol{\Sigma}_k|^{-\frac{1}{2}} \exp\left[-\frac{1}{2} (\mathbf{t}_p - \boldsymbol{\psi}_k)^T \boldsymbol{\Sigma}_k^{-1} (\mathbf{t}_p - \boldsymbol{\psi}_k)\right]. \end{aligned} \quad (34)$$

Unfortunately, it is too difficult to generate samples distributed according to (33) or (34). Therefore, a Metropolis-Hastings step is used, based on a random walk method [30, p. 245] with a Gaussian distribution  $\mathcal{N}(0, u_r^2)$  as proposal distribution. The variance  $u_r^2$  of the instrumental distribution has been fixed to obtain an acceptance rate between 0.15 and 0.5 as recommended in [31].

### C. Conditional distributions of endmember/noise variances

For each pixel  $p$ , the Bayes theorem yields

$$f(s_p^2 | \mathbf{y}_p, \mathbf{t}_p, \delta) \propto f(\mathbf{y}_p | \mathbf{t}_p, s_p^2) f(s_p^2 | \delta).$$

As a consequence, the following results can be obtained

1) *LMM*:  $s_p^2 | \mathbf{y}_p, \mathbf{t}_p, \delta$  is distributed according to the inverse-Gamma distribution

$$s_p^2 | \mathbf{y}_p, \mathbf{t}_p, \delta \sim \mathcal{IG}\left(\frac{L}{2} + 1, \frac{\|\mathbf{y}_p - \mathbf{M}\mathbf{a}_p(\mathbf{t}_p)\|^2}{2} + \delta\right). \quad (35)$$

<sup>2</sup>The noise or endmember variances have been omitted for sake of conciseness.

2) *NCM*: the conditional distribution of  $w_p^2 | \mathbf{y}_p, \mathbf{t}_p, \delta$  is the inverse-Gamma distribution

$$w_p^2 | \mathbf{y}_p, \mathbf{t}_p, \delta \sim \mathcal{IG} \left( \frac{L}{2} + 1, \frac{\|\mathbf{y}_p - \boldsymbol{\mu}(\mathbf{t}_p)\|^2}{2c(\mathbf{t}_p)} + \delta \right). \quad (36)$$

#### D. Conditional distribution of $\Psi$ and $\Sigma$

The conditional distributions of the two hyperparameters  $\Psi$  and  $\Sigma$  are the same for the LMM and NCM. For each endmember  $r$  ( $r = 1, \dots, R$ ) and each class  $k$  ( $k = 1, \dots, K$ ), thanks to Bayes relation the conditional distribution of  $\psi_{r,k}$  can be written as

$$f(\psi_{r,k} | \mathbf{z} = k, \mathbf{t}_r, \sigma_{r,k}^2, v^2) \propto f(\psi_{r,k} | v^2) \prod_{p \in \mathcal{I}_k} f(t_{r,p} | z_p = k, \psi_{r,k}, \sigma_{r,k}^2). \quad (37)$$

Similarly, the conditional distribution of  $\sigma_{r,k}^2$  is

$$f(\sigma_{r,k}^2 | \mathbf{t}_r, \mathbf{z} = k, \psi_{r,k}) \propto f(\sigma_{r,k}^2) \prod_{p \in \mathcal{I}_k} f(t_{r,p} | z_p = k, \psi_{r,k}, \sigma_{r,k}^2). \quad (38)$$

Straightforward computations allow one to obtain the following results

$$\psi_{r,k} | \mathbf{z} = k, \mathbf{t}_r, \sigma_{r,k}^2, v^2 \sim \mathcal{N} \left( \frac{v^2 n_k \bar{t}_{r,k}}{\sigma_{r,k}^2 + v^2 n_k}, \frac{v^2 \sigma_{r,k}^2}{\sigma_{r,k}^2 + v^2 n_k} \right) \quad (39)$$

with  $\bar{t}_{r,k} = \frac{1}{n_k} \sum_{p \in \mathcal{I}_k} t_{r,p}$  and

$$\sigma_{r,k}^2 | \mathbf{z} = k, \mathbf{t}_r, \psi_{r,k} \sim \mathcal{IG} \left( \frac{n_k}{2} + 1, \gamma + \sum_{p \in \mathcal{I}_k} \frac{(t_{r,p} - \psi_{r,k})^2}{2} \right). \quad (40)$$

#### E. Conditional distribution of $v^2$ and $\delta$

The conditional distribution of  $v^2$  is the following inverse-gamma distribution

$$v^2 | \Psi \sim \mathcal{IG} \left( \frac{RK}{2}, \frac{1}{2} \Psi^T \Psi \right). \quad (41)$$

whereas the posterior distribution of  $\delta$  differs for the LMM and NCM

1) *LMM*:

$$\delta | \mathbf{s} \sim \mathcal{G} \left( P, \sum_{p=1}^P \frac{1}{s_p^2} \right) \quad (42)$$

2) *NCM*:

$$\delta | \mathbf{w} \sim \mathcal{G} \left( P, \sum_{p=1}^P \frac{1}{w_p^2} \right). \quad (43)$$



---

**Algorithm 2** Hybrid Gibbs sampler for hyperspectral unmixing using spatial constraints for the NCM

---

```

1: % Initialization:
2: Sample  $\mathbf{z}^{(0)}$  from probability density function (pdf) in Eq. (16),
3: Sample  $\delta^{(0)}$  and  $v^{2(0)}$  from the pdfs in Eq. (27),
4: Sample  $\mathbf{w}^{(0)}$  from the pdf in Eq. (21),
5: Sample  $\Psi^{(0)}$  from the pdf in Eq. (25),
6: Sample  $\Sigma^{(0)}$  from the pdf in Eq. (26),
7: % Iterations:
8: for  $t = 1, 2, \dots$  do
9:   for each pixel  $p = 1, \dots, P$  do
10:     Sample  $\mathbf{z}^{(t)}$  from the pdf in Eq. (32),
11:     Sample  $\mathbf{t}_p^{(t)}$  from the pdf in Eq. (33) using Metropolis-within-Gibbs step,
12:     Set  $\mathbf{a}_p^{(t)}$  from Eq. (9),
13:     Sample  $w_p^{2(t)}$  from the pdf in Eq. (36),
14:   end for
15:   for each class  $k = 1, \dots, K$  do
16:     for each endmember  $r = 1, \dots, R$  do
17:       Sample  $\psi_{r,k}^{(t)}$  from the pdf in Eq. (39),
18:       Sample  $\sigma_{r,k}^{2(t)}$  from the pdf in Eq. (40),
19:     end for
20:   end for
21:   Sample  $v^{2(t)}$  from the pdf in Eq. (41)
22:   Sample  $\delta^{(t)}$  from the pdf in Eq. (43),
23: end for

```

---

## V. SIMULATION RESULTS ON SYNTHETIC DATA

Many simulations have been conducted to illustrate the accuracy of the proposed algorithms. The first experiment considers a  $25 \times 25$  synthetic image with  $K = 3$  different classes. The image contains  $R = 3$  mixed components whose spectra ( $L = 413$  spectral bands) have been extracted from the spectral libraries distributed with the ENVI package [32] and are represented in Fig. 4. A label map shown in Fig. 5 (left) has been generated

---

**Algorithm 3** Hybrid Gibbs sampler for hyperspectral unmixing using spatial constraints for the LMM

---

```

1: % Initialization:
2: Sample  $\mathbf{z}^{(0)}$  from probability density function (pdf) in Eq. (16),
3: Sample  $\delta^{(0)}$  and  $v^{2(0)}$  from the pdfs in Eq. (27),
4: Sample  $\mathbf{s}^{(0)}$  from the pdf in Eq. (22),
5: Sample  $\Psi^{(0)}$  from the pdf in Eq. (25),
6: Sample  $\Sigma^{(0)}$  from the pdf in Eq. (26),
7: % Iterations:
8: for  $t = 1, 2, \dots$  do
9:   for each pixel  $p = 1, \dots, P$  do
10:     Sample  $\mathbf{z}^{(t)}$  from the pdf in Eq. (32),
11:     Sample  $\mathbf{t}_p^{(t)}$  from the pdf in Eq. (33) using Metropolis-within-Gibbs step,
12:     Set  $\mathbf{a}_p^{(t)}$  from Eq. (9),
13:     Sample  $s_p^{2(t)}$  from the pdf in Eq. (35),
14:   end for
15:   for each class  $k = 1, \dots, K$  do
16:     for each endmember  $r = 1, \dots, R$  do
17:       Sample  $\psi_{r,k}^{(t)}$  from the pdf in Eq. (39),
18:       Sample  $\sigma_{r,k}^{2(t)}$  from the pdf in Eq. (40),
19:     end for
20:   end for
21:   Sample  $v^{2(t)}$  from the pdf in Eq. (41)
22:   Sample  $\delta^{(t)}$  from the pdf in Eq. (42),
23: end for

```

---

using (16) with  $\beta = 1.1$ .

The mean and variance of the abundances have been chosen for each class as reported in Table I. These values reflect the fact that the 1st endmember is more present in Class 1 (with average concentration of 60%), the 2nd endmember is more present in Class 2 (with average concentration of 50%) and the 3rd endmember is more present in Class 3 (with average concentration of 50%). In this simulation scenario, the abundance variance has been fixed to a common value 0.005 for all endmembers, pixels and classes. The generated abundance

TABLE I  
ACTUAL AND ESTIMATED ABUNDANCE MEAN AND VARIANCE IN EACH CLASS.

	Class 1		Class 2		Class 3	
	$\mu_1 = E[a_p]$	$\text{Var}[a_{p,r}]$	$\mu_2 = E[a_p]$	$\text{Var}[a_{p,r}]$	$\mu_3 = E[a_p]$	$\text{Var}[a_{p,r}]$
Actual values	$[0.6, 0.3, 0.1]^T$	0.005	$[0.3, 0.5, 0.2]^T$	0.005	$[0.3, 0.2, 0.5]^T$	0.005
Estimated values (LMM)	$[0.58, 0.29, 0.13]^T$	0.0047	$[0.29, 0.49, 0.2]^T$	0.0055	$[0.31, 0.19, 0.49]^T$	0.0076
Estimated values (NCM)	$[0.59, 0.29, 0.12]^T$	0.0055	$[0.31, 0.49, 0.2]^T$	0.007	$[0.31, 0.2, 0.49]^T$	0.007

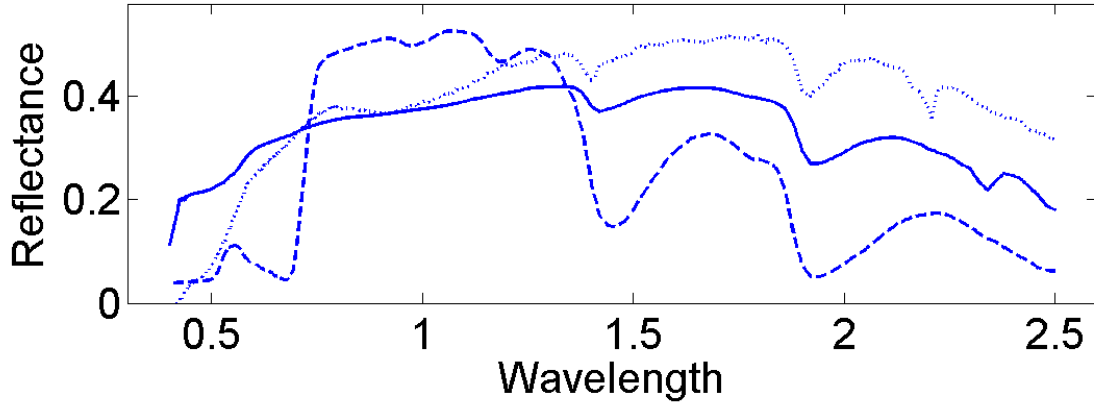


Fig. 4. The  $R = 3$  endmember spectra: construction concrete (solid line), green grass (dashed line), micaceous loam (dotted line).

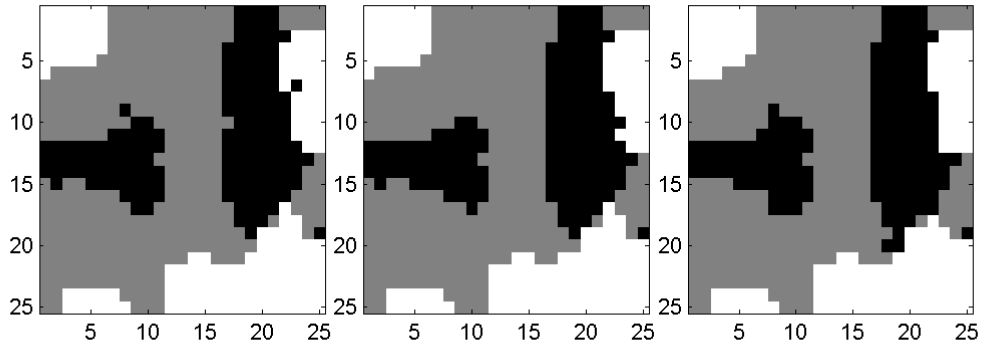


Fig. 5. Left: the actual label map. Center: the label map estimated by the LMM hybrid Gibbs sampler. Right: the label map estimated by the NCM hybrid Gibbs sampler.

maps for the LMM and NCM are depicted in Fig. 6 (top) and Fig. 7 (top), respectively. Note that a white (resp. black) pixel in the fraction map indicates a large (resp. small) value of the abundance coefficient. The noise and endmember variances are generated according to their prior distribution (22) and (21) with  $\delta = 1 \times 10^{-3}$  leading to the following signal-to-noise ratios (SNR): (LMM)  $\text{SNR}_{\text{LMM}} = 19\text{dB}$  and (NCM)  $\text{SNR}_{\text{NCM}} = 12\text{dB}$ .

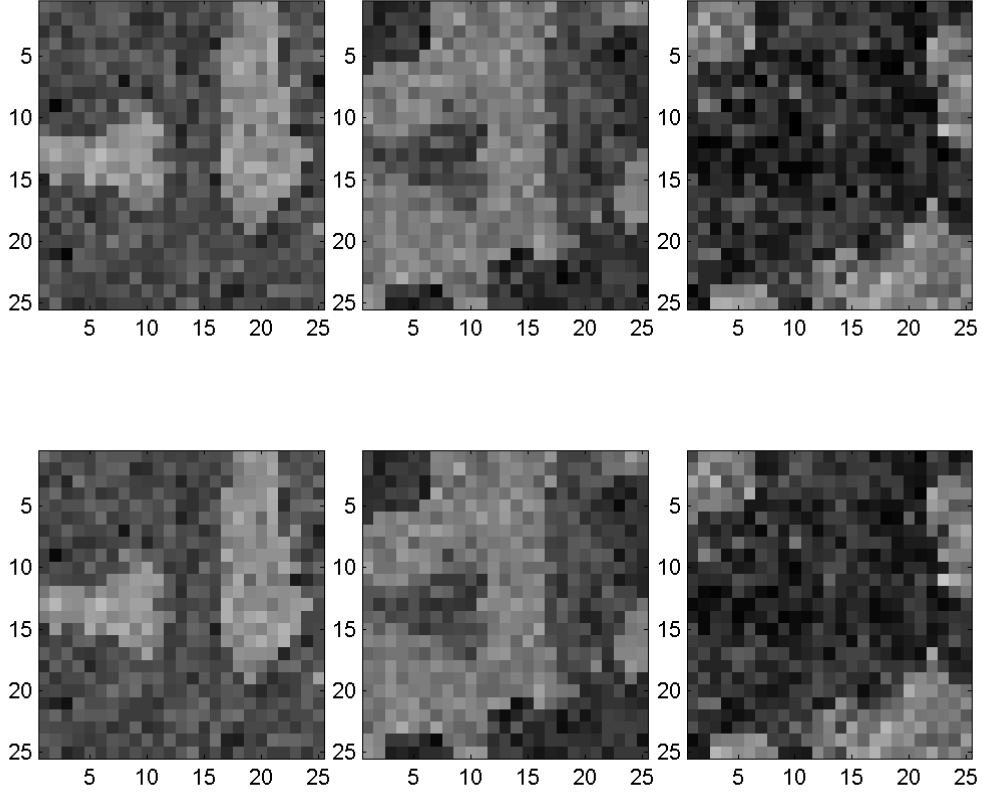


Fig. 6. Top: abundance maps of the 3 pure materials for LMM. Bottom: abundance maps of the 3 pure materials estimated by the LMM-based hybrid Gibbs sampler (from left to right: construction concrete, green grass, micaceous loam).

The MMSE and MAP estimators of the unknown parameters can be computed from samples generated with the Gibbs samplers presented in Section IV. For instance, the marginal MAP estimates of the label vector  $\hat{z}_{\text{MAP}}$  are depicted in Fig. 5 for both the LMM- and NCM-based hybrid Gibbs algorithms (center and right). The corresponding MMSE estimates of the abundances conditioned upon  $\hat{z}_{\text{MAP}}$  have been also shown in Fig. 6 (bottom) and 7 (bottom) for both models. A number of  $N_{\text{MC}} = 5000$  iterations (with 500 burn-in iterations) has been necessary to obtain these results. Moreover, as mentioned in Section IV, the proposed algorithms generate samples distributed according to the full posteriors of interest. Then, these

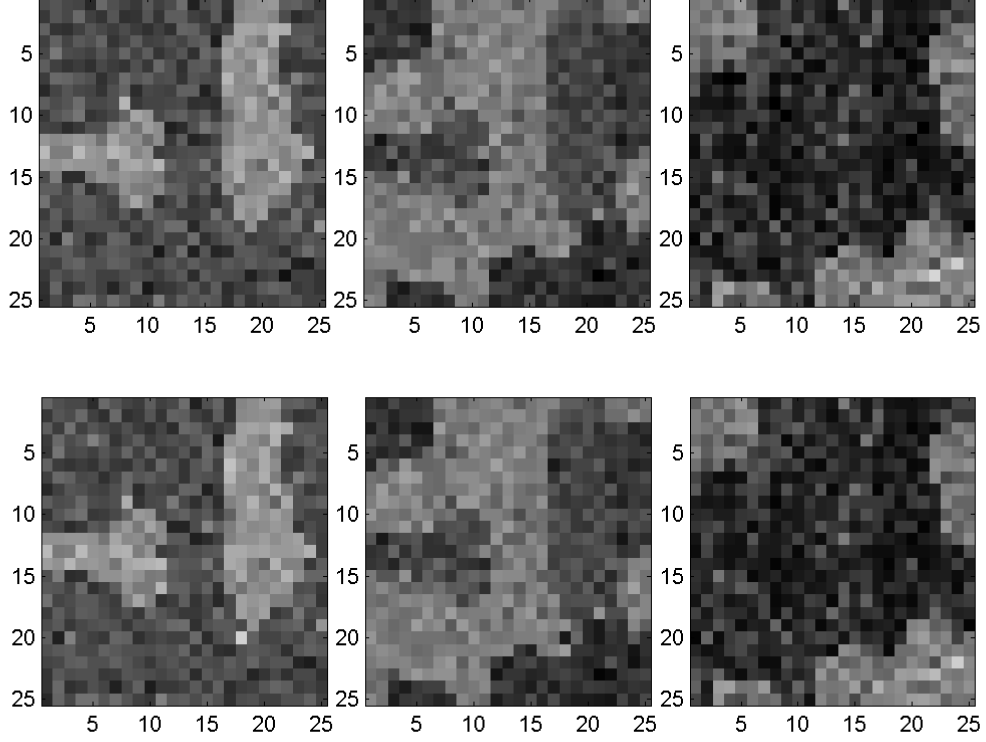


Fig. 7. Top: abundance maps of the 3 pure materials for NCM. Bottom: abundance maps of the 3 pure materials estimated by the LMM-based hybrid Gibbs sampler (from left to right: construction concrete, green grass, micaceous loam).

samples can be used to compute, for instance, the posterior distributions of the mean vectors  $\boldsymbol{\mu}_k = \mathbb{E}[\mathbf{a}_p]$  ( $k = 1, \dots, K$ ,  $p \in \mathcal{I}_k$ ). These mean vectors, introduced in (5), are of great interest since they are characteristics of each class  $k = 1, \dots, K$ , according to their definition in paragraph II-B. Therefore, as an additional insight, the histograms of the abundance means  $\boldsymbol{\mu}_k$  estimated by the proposed algorithms have been depicted in Fig. 8 for the 2nd class, i.e.,  $k = 2$ . Similar results have been obtained for the other classes. They are omitted here for brevity. Finally, the estimated abundance means and variances for each endmember in each class have been reported in Table I (last row). The estimated classes, abundance coefficients and abundance mean vectors estimated by both algorithms are clearly in accordance with the actual ones.

The LMM and NCM hybrid Gibbs algorithm are compared respectively to their non-spatial constrained Bayesian counterpart developed in [9] and [33], respectively. The synthetic image shown in Fig. 5 has been analyzed by the initial algorithms of [9] and [33] with the same number of iterations  $N_{MC}$  in addition with the FCLS [7] algorithm. As a criterion, the global

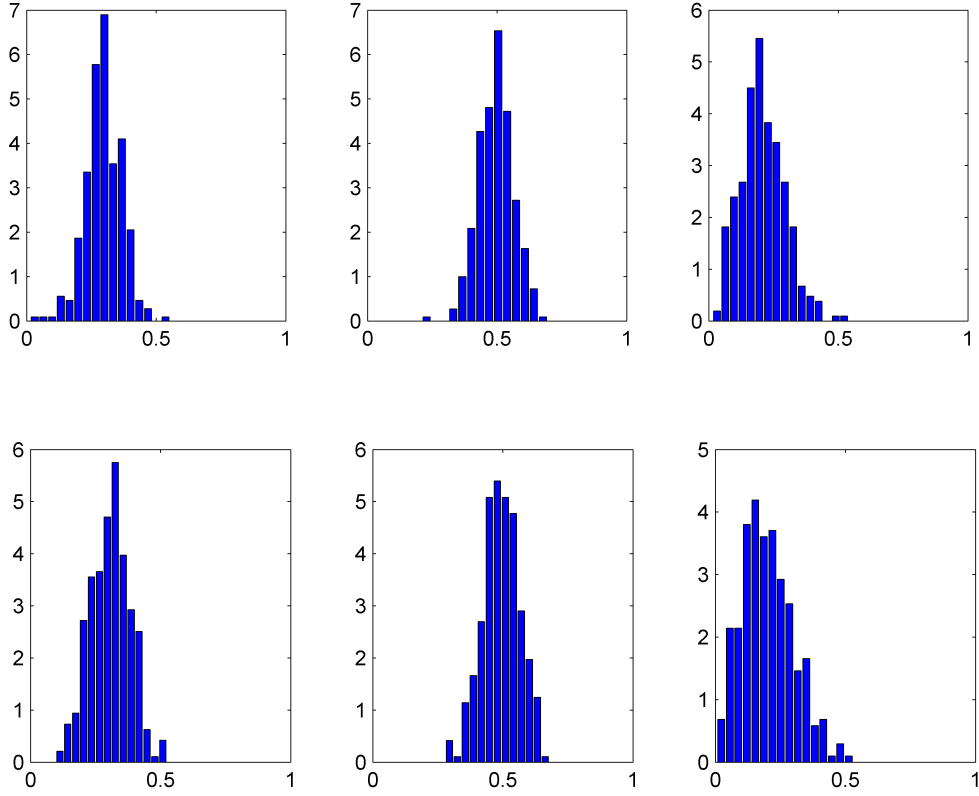


Fig. 8. Top (resp. bottom): histograms of the abundance means  $\boldsymbol{\mu}_k = [\mu_{k,1}, \mu_{k,2}, \mu_{k,3}]^T$  estimated by the LMM-based (resp. NCM-based) hybrid Gibbs algorithm for the 2nd class ( $k = 2$ ).

mean square error (MSE) of the  $r$ th estimated abundances have been computed for each algorithm. This global MSE is defined as

$$\text{MSE}_r^2 = \frac{1}{P} \sum_{p=1}^P (\hat{a}_{r,p} - a_{r,p})^2 \quad (44)$$

where  $\hat{a}_{r,p}$  denotes the MMSE estimate of the abundance  $a_{r,p}$ . Table II reports the different results showing that the algorithms developed in this paper (referred to as “Spatial”) perform better than the non-spatial constrained algorithms (referred to as “Bayesian” and “FCLS”).

## VI. SIMULATION RESULTS ON AN AVIRIS IMAGE

This section illustrates the performance of the proposed spatial algorithms on a real hyper-spectral dataset, acquired over Moffett Field (CA, USA) in 1997 by the JPL spectro-imager AVIRIS. Many previous works have used this image to illustrate and compare algorithm performance with hyperspectral images [34], [35]. The region of interest is a  $50 \times 50$  pixel

TABLE II  
GLOBAL MSEs OF EACH ABUNDANCE COMPONENT.

	NCM		LMM		
	Bayesian	Spatial	FCLS	Bayesian	Spatial
$MSE_1^2$	0.0027	0.0013	0.0019	0.0016	0.001
$MSE_2^2$	$8.9 \times 10^{-4}$	$5.9 \times 10^{-4}$	$4.3 \times 10^{-4}$	$4.1 \times 10^{-4}$	$3.1 \times 10^{-4}$
$MSE_3^2$	$9.5 \times 10^{-4}$	$5.5 \times 10^{-4}$	0.0014	0.0013	$8.6 \times 10^{-4}$

image, represented in Fig. 9. The data set has been reduced from the original 224 bands to  $L = 189$  bands by removing water absorption bands. As in [9], a principal component analysis has been conducted as a processing step to determine the number of endmembers present in the scene. Then, the endmembers spectra have been extracted with the help of the endmember extraction procedure N-FINDR proposed by Winter in [36]. The  $R = 3$  extracted endmembers, shown in Fig. 10, corresponds to soil, vegetation and water. The algorithms proposed in Section IV have been applied on this image with a number of  $K = 4$  classes and  $N_{MC} = 5000$  iterations (with 500 burn-in iterations).

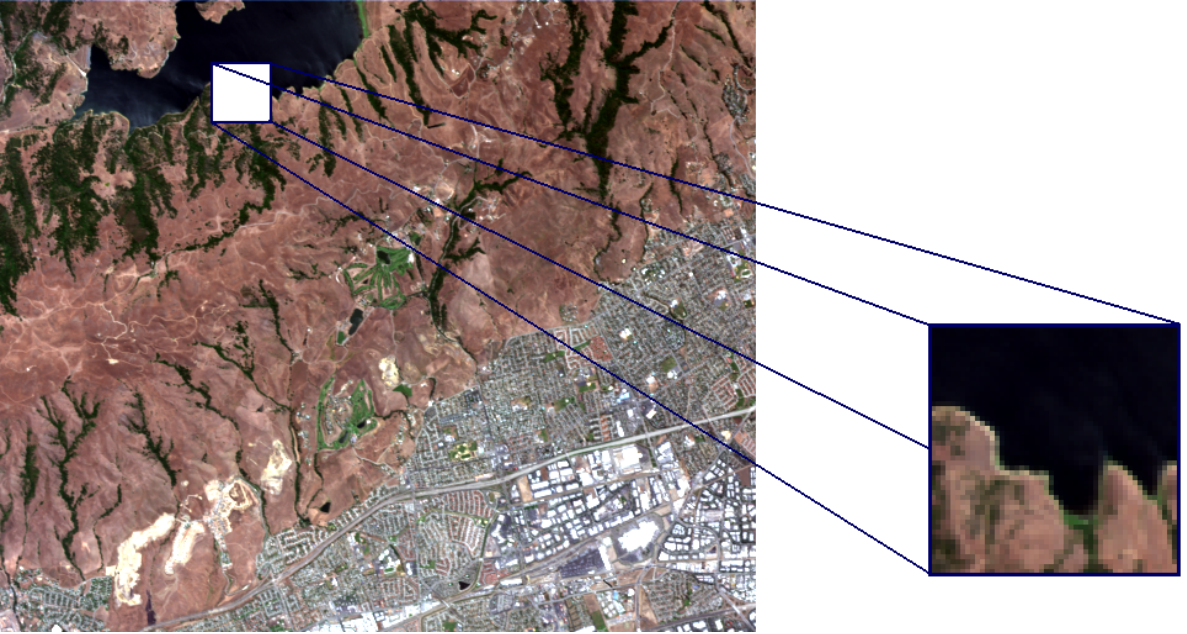


Fig. 9. Real hyperspectral data: Moffett field acquired by AVIRIS in 1997 (left) and the region of interest shown in true colors (right).

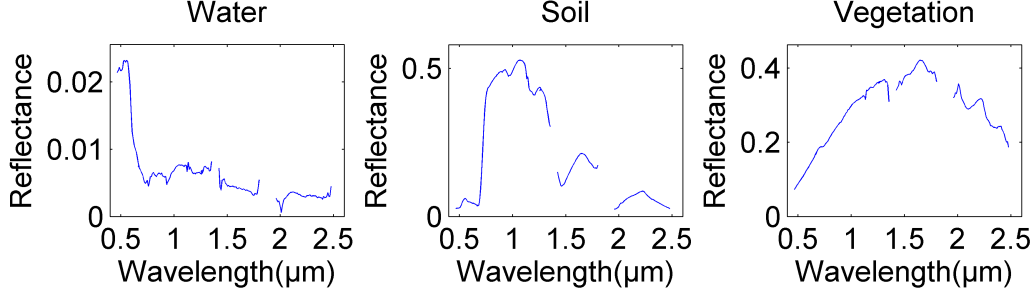


Fig. 10. The  $R = 3$  endmember spectra obtained by the N-FINDR algorithm.

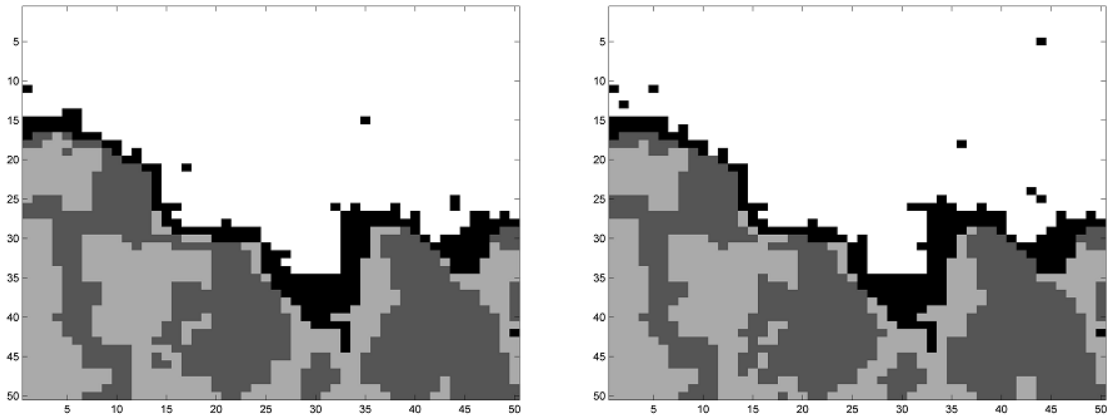


Fig. 11. Left (resp. right): label maps estimated by the proposed LMM-based (resp. NCM-based) algorithm.

The estimated classification and abundance maps for the LMM- and NCM-based hybrid Gibbs algorithms are respectively depicted in Fig. 11 and 12. The results provided by both algorithms are very similar and in good agreement with results represented in Fig. 13 and obtained on this image with an LMM-based Bayesian algorithm [9] or with the well-known FCLS algorithm [7].

## VII. CONCLUSIONS

A new hierarchical Bayesian algorithm was proposed for unmixing hyperspectral images. Markov random fields were introduced to model spatial correlations between the pixels of the image. An additional hidden discrete variable (label) was introduced to identify several classes defined by homogeneous abundances (with constant first and second order statistics). The positivity and sum-to-one constraints on the abundances were handled by using an appropriate



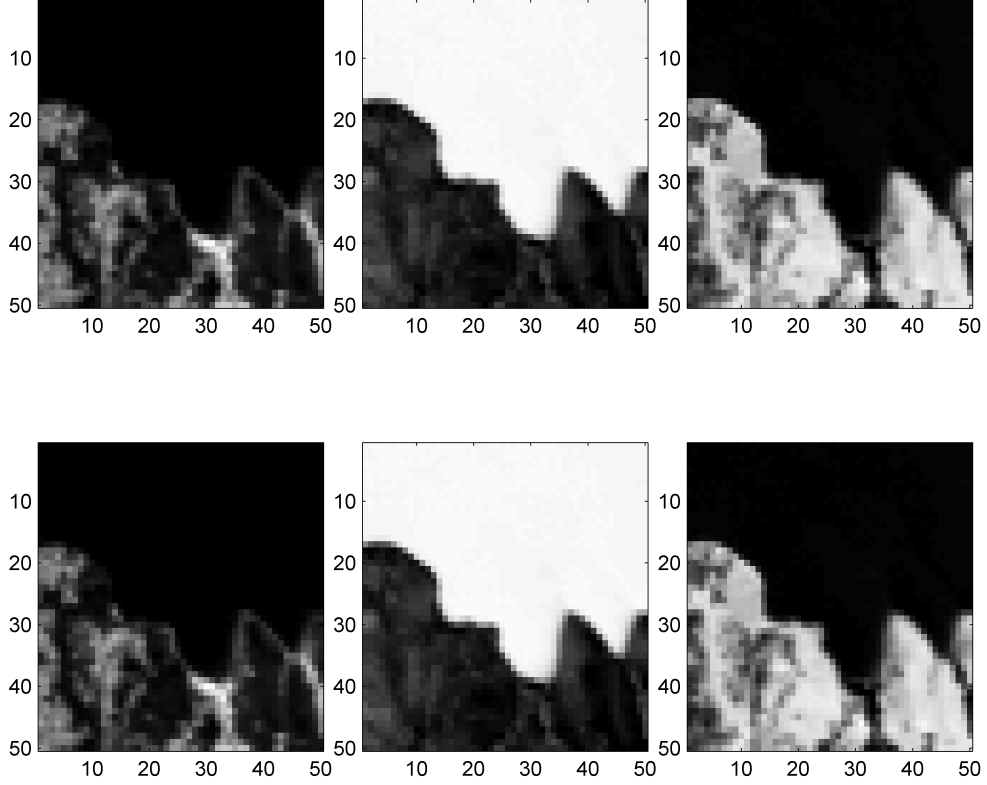


Fig. 12. Top (resp. bottom): abundance maps estimated by the proposed LMM-based (resp. NCM-based) algorithm (from left to right: vegetation, water and soil).

reparametrization defined by logistic coefficient vectors. We derived the joint posterior distributions of the unknown parameters and hyperparameters associated to the proposed Bayesian linear mixing model and normal compositional model. Two MCMC methods were studied to generate samples asymptotically distributed according to the posterior distribution associated to these two models. The generated samples were then used to estimate the abundance maps as well as the underlying image labels. The results obtained on simulated data and on a real AVIRIS image are interesting. Perspectives include the estimation of the granularity coefficient involved in Potts-Markov random fields.

## REFERENCES

- [1] K. Jusoff, "Precision forestry using airborne hyperspectral imaging sensor," *Journal of Agricultural Science*, vol. 1, no. 1, pp. 142–147, June 2009.
- [2] N. Keshava and J. Mustard, "Spectral unmixing," *IEEE Signal Processing Magazine*, pp. 44–56, Jan. 2002.
- [3] C.-I Chang, *Hyperspectral data exploitation: theory and applications*. Hoboken, NJ: Wiley, 2007.

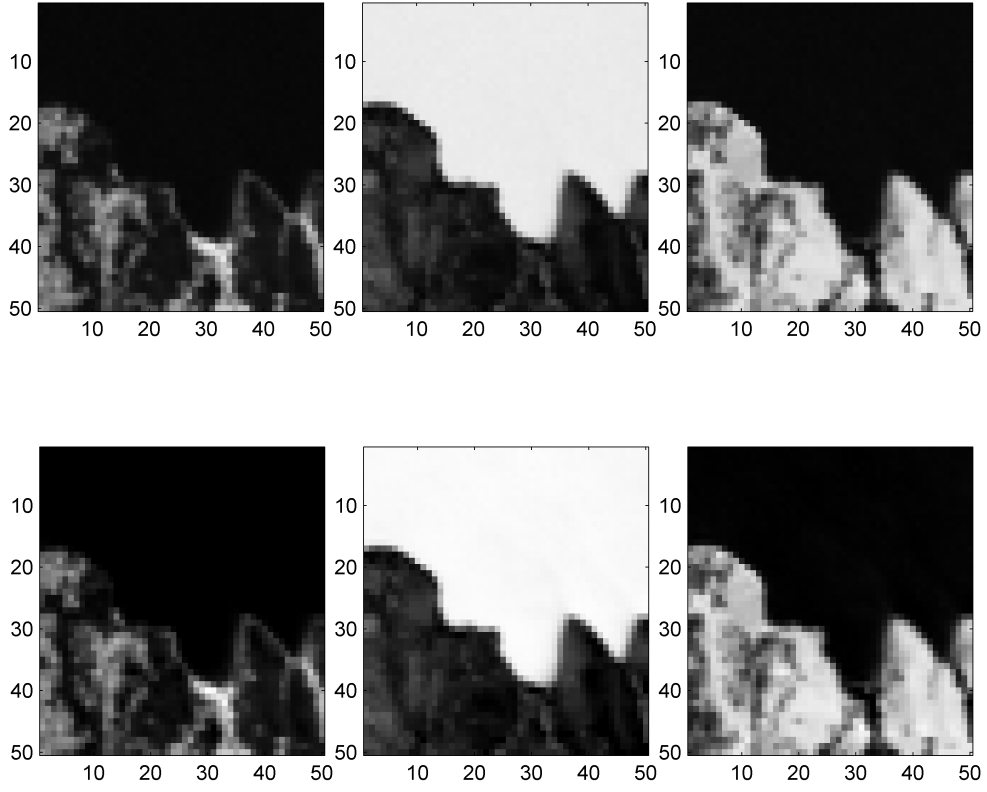


Fig. 13. Top: abundance maps estimated by the LMM-based Bayesian algorithm (from [9]). Bottom: fraction maps estimated by the FCLS algorithm [7].

- [4] M. T. Eismann and D. Stein, “Stochastic mixture modeling,” in *Hyperspectral Data Exploitation: Theory and Applications*, C.-I Chang, Ed. Wiley, 2007, ch. 5.
- [5] O. Eches, N. Dobigeon, and J.-Y. Tournet, “NCM-based Bayesian algorithm for hyperspectral unmixing,” in *Proc. IEEE GRSS Workshop on Hyperspectral Image and Signal Processing: Evolution in Remote Sensing (WHISPERS)*, Grenoble, France, Aug. 2009, pp. 1–4.
- [6] P. J. Martinez, R. M. Perez, A. Plaza, P. L. Aguilar, M. C. Cantero, and J. Plaza, “Endmember extraction algorithms from hyperspectral images,” *Annals of Geophysics*, vol. 49, no. 1, pp. 93–101, Feb. 2006.
- [7] D. C. Heinz and C.-I Chang, “Fully constrained least squares linear spectral mixture analysis method for material quantification in hyperspectral imagery,” *IEEE Trans. Geosci. and Remote Sensing*, vol. 39, no. 3, pp. 529–545, March 2001.
- [8] C. Theys, N. Dobigeon, J.-Y. Tournet, and H. Lantéri, “Linear unmixing of hyperspectral images using a scaled gradient method,” in *Proc. IEEE-SP Workshop Stat. and Signal Processing (SSP)*, Cardiff, UK, Aug. 2009, pp. 729–732.
- [9] N. Dobigeon, J.-Y. Tournet, and C.-I Chang, “Semi-supervised linear spectral using a hierarchical Bayesian model for hyperspectral imagery,” *IEEE Trans. Signal Processing*, vol. 56, no. 7, pp. 2684–2696, July 2008.
- [10] J. Besag, “Spatial interaction and the statistical analysis of lattice systems,” *J. Roy. Stat. Soc. Ser. B*, vol. 36, no. 2, pp. 192–236, 1974.

- [11] S. Geman and D. Geman, "Stochastic relaxation, Gibbs distributions, and the Bayesian restoration of images," *IEEE Trans. Patt. Anal. Mach. Intell.*, vol. 6, no. 6, pp. 721–741, Nov. 1984.
- [12] A. Mohammadpour, O. Féron, and A. Mohammad-Djafari, "Bayesian segmentation of hyperspectral images," in *Proc. Workshop on Bayesian Inference and Maximum Entropy Methods (MaxEnt)*, ser. AIP Conference Series, R. Fischer, R. Preuss, and U. V. Toussaint, Eds., vol. 735, Max Plank Inst., Germany, Nov. 2004, pp. 541–548.
- [13] R. Neher and A. Srivastava, "A Bayesian MRF framework for labeling terrain using hyperspectral imaging," *IEEE Trans. Geosci. and Remote Sensing*, vol. 43, no. 6, pp. 1363–1374, June 2005.
- [14] G. Rellier, X. Descombes, F. Falzon, and J. Zerubia, "Texture feature analysis using a Gauss-Markov model in hyperspectral image classification," *IEEE Trans. Geosci. and Remote Sensing*, vol. 42, no. 7, pp. 1543–1551, July 2004.
- [15] N. Bali and A. Mohammad-Djafari, "Bayesian approach with hidden Markov modeling and mean field approximation for hyperspectral data analysis," *IEEE Trans. Image Processing*, vol. 17, no. 2, pp. 217–225, Feb. 2008.
- [16] F. Wu, "The Potts model," *Rev. Modern Phys.*, vol. 54, no. 1, pp. 235–268, Jan. 1982.
- [17] N. Dobigeon, S. Moussaoui, M. Coulon, J.-Y. Tourneret, and A. O. Hero, "Joint Bayesian endmember extraction and linear unmixing for hyperspectral imagery," *IEEE Trans. Signal Processing*, vol. 57, no. 11, pp. 4355–4368, Nov. 2009.
- [18] C. Kevrann and F. Heitz, "A Markov random field model-based approach to unsupervised texture segmentation using local and global statistics," *IEEE Trans. Image Processing*, vol. 4, no. 6, pp. 856–862, June 1995.
- [19] A. Tonazzini, L. Bedini, and E. Salerno, "A Markov model for blind image separation by a mean-field EM algorithm," *IEEE Trans. Image Processing*, vol. 15, no. 2, pp. 473–481, Feb. 2006.
- [20] R. S. Rand and D. M. Keenan, "Spatially smooth partitioning of hyperspectral imagery using spectral/spatial measures of disparity," *IEEE Trans. Geosci. and Remote Sensing*, vol. 41, no. 6, pp. 1479–1490, June 2003.
- [21] R. Kindermann and J. L. Snell, *Markov random fields and their applications*. Providence, RI: Amer. Math. Soc., 1980.
- [22] J.-M. Marin and C. P. Robert, *Bayesian core: a practical approach to computational Bayesian statistics*. New-York: Springer, 2007.
- [23] Z. Zhou, R. Leahy, and J. Qi, "Approximate maximum likelihood hyperparameter estimation for Gibbs prior," *IEEE Trans. Image Processing*, vol. 6, no. 6, pp. 844–861, June 1997.
- [24] X. Descombes, R. Morris, J. Zerubia, and M. Berthod, "Estimation of Markov random field prior parameters using Markov chain Monte Carlo maximum likelihood," *IEEE Trans. Image Processing*, vol. 8, no. 7, pp. 945–963, July 1999.
- [25] G. Celeux, F. Forbes, and N. Peyrard, "EM procedures using mean field-like approximations for Markov model-based image segmentation," *Pattern Recognition*, vol. 36, no. 1, pp. 131–144, 2003.
- [26] A. Gelman, F. Bois, and J. Jiang, "Physiological pharmacokinetic analysis using population modeling and informative prior distributions," *J. Amer. Math. Soc.*, vol. 91, no. 436, pp. 1400–1412, Dec. 1996.
- [27] K. Themelis and A. A. Rontogiannis, "A soft constrained MAP estimator for supervised hyperspectral signal unmixing," in *Proc. of European Signal Processing Conf. (EUSIPCO)*, Lausanne, Switzerland, Aug. 2008.
- [28] E. Punskeya, C. Andrieu, A. Doucet, and W. Fitzgerald, "Bayesian curve fitting using MCMC with applications to signal segmentation," *IEEE Trans. Signal Processing*, vol. 50, no. 3, pp. 747–758, March 2002.
- [29] N. Dobigeon, J.-Y. Tourneret, and M. Davy, "Joint segmentation of piecewise constant autoregressive processes by using a hierarchical model and a Bayesian sampling approach," *IEEE Trans. Signal Processing*, vol. 55, no. 4, pp. 1251–1263, April 2007.
- [30] C. P. Robert and G. Casella, *Monte Carlo Statistical Methods*, 2nd ed. New York: Springer Verlag, 2004.

- [31] G. O. Roberts, “Markov chain concepts related to sampling algorithms,” in *Markov Chain Monte Carlo in Practice*, W. R. Gilks, S. Richardson, and D. J. Spiegelhalter, Eds. London: Chapman & Hall, 1996, pp. 259–273.
- [32] RSI (Research Systems Inc.), *ENVI User’s guide Version 4.0*, Boulder, CO 80301 USA, Sept. 2003.
- [33] O. Eches, N. Dobigeon, C. Mailhes, and J.-Y. Tourneret, “Unmixing hyperspectral images using a normal compositional model and MCMC methods,” *IEEE Trans. Image Processing*, 2010, to appear.
- [34] E. Christophe, D. Léger, and C. Mailhes, “Quality criteria benchmark for hyperspectral imagery,” *IEEE Trans. Geosci. and Remote Sensing*, vol. 43, no. 9, pp. 2103–2114, Sept. 2005.
- [35] T. Akgun, Y. Altunbasak, and R. M. Mersereau, “Super-resolution reconstruction of hyperspectral images,” *IEEE Trans. Image Processing*, vol. 14, no. 11, pp. 1860–1875, Nov. 2005.
- [36] M. E. Winter, “Fast autonomous spectral endmember determination in hyperspectral data,” in *Proc. 13th Int. Conf. on Applied Geologic Remote Sensing*, vol. 2, Vancouver, April 1999, pp. 337–344.